Optics Letters

# Transport of light in a moving photonic lattice via atomic coherence

Zhaoyang Zhang,[1,*] Yutong Shen,[1] Shaohuan Ning,[1] Shun Liang,[1] Yuan Feng,[1] Changbiao Li,[1] Yanpeng Zhang,[1] and Min Xiao[2,3]

[1]Key Laboratory for Physical Electronics and Devices of the Ministry of Education & Shaanxi Key Lab of Information Photonic Technique, School of Electronic Science and Engineering, Faculty of Electronic and Information Engineering, Xi'an Jiaotong University, Xi'an 710049, China
[2]Department of Physics, University of Arkansas, Fayetteville, Arkansas 72701, USA
[3]National Laboratory of Solid State Microstructures and School of Physics, Nanjing University, Nanjing 210093, China
*Corresponding author: zhyzhang@xjtu.edu.cn

Received 14 June 2021; revised 16 July 2021; accepted 16 July 2021; posted 19 July 2021 (Doc. ID 434164); published 18 August 2021

**In this Letter, we have investigated experimentally the photonic realization of a moving lattice with an instantaneously tunable transverse velocity in a three-level Λ-type warm $^{85}$Rb atomic medium. The dynamic photonic lattice moving along the direction of its spatial periodicity was constructed by introducing a frequency difference (determining the velocity) between two coupling beams, whose interference pattern could optically induce a (spatial) periodic refractive index change inside the atomic vapor under electromagnetically induced transparency. When a Gaussian probe field is launched into this optically induced lattice, the output diffraction patterns can shift along the transverse direction, indicating dynamical features of induced photonic structures. The realization of this effectively controllable moving photonic lattice provides a new platform for guiding the transport of light.** 

https://doi.org/10.1364/OL.434164

Engineering photonic waveguides periodically can form photonic lattices with desired dispersive band structures so that the spatial transport of light in photonic lattices exhibits a rather unique advantage of directly mapping the temporal evolutions of wave function in semiconductor crystals [1–3]. During past few decades, great research efforts have been made to investigate the interactions between light and linear/nonlinear photonic lattices, and a variety of remarkable optical properties have been demonstrated, including non-Hermitian phase transition [4–6], photonic topological insulators and topological lasing [7–9], localized states [10,11], and edge states [12,13]. To date, the capability of manipulating light waves using photonic lattices is still a current topic, and waveguides are arranged in different geometries to form peculiar photonic band structures. Recent studies have further extended research to super-honeycomb lattices: hybrid fermionic and bosonic systems [14,15], sawtooth lattices with non-diffractive flat bands [16,17], Moire lattices composed of two periodic photonic structures [10,18], and even photonic lattices with synthetic dimensions [19].

Most of the earlier works included static photonic lattices, while the unique properties of moving photonic lattices remain to be explored further. Compared to traditional stationary periodic structures, one interesting feature in a one-dimensional moving photonic lattice (with a speed along the direction of its spatial periodicity) is that the band gap can dynamically shift to a different frequency range by controlling the moving velocity [20]. In addition, the light travelling in a linear moving photonic lattice may exhibit intriguing phenomena akin to nonlinear effects under relativistic condition [21]. For example, a moving photonic lattice was constructed in a coherently prepared multi-level atomic system, and by measuring the output reflection and transmission spectra, optical isolation is clearly and visually demonstrated with the assistance of the relativistic Doppler effect [22]. This kind of dynamic photonic lattices is established by optically moving a standing-wave pattern (by detuning the two counter-propagating components forming the standing wave slightly) under electromagnetically induced transparency (EIT) [23], instead of mechanically moving any physical components forming the setup. Motivated by that early work, the discrete transport dynamics is theoretically predicted in a moving photonic lattice in a coherent atomic gas [24], which opens the door for demonstrating the discrete characteristics of optical waves in dynamic photonic lattices formed in coherent multi-level atomic media.

Following the recent advances, such as parity-time symmetry [25] and spin-orbit coupling based on pseudospin [26,27], in static photonic lattices induced in EIT atomic systems [12,28–30], we experimentally demonstrate the discrete dynamic characteristics of a Gaussian probe beam passing through a moving photonic lattice, established in a three-level rubidium atomic vapor system. A coherent multi-level atomic medium allows *in situ* reconfigurability of an optically induced lattice, thus enabling the construction of a rapidly adjustable moving photonic lattice. The transverse speed of the lattice is introduced by a slight frequency difference between the two coupling laser beams, whose interference pattern modulates the refractive index in a spatially periodic manner under the EIT condition. As a result, the output of the incident probe beam exhibits discrete spatial patterns with the same periodicity as the formed standing wave. By controlling the frequency difference to effectively manipulate the moving velocity of the photonic

lattice, the motion of the output-discretized probe field is clearly observed along the direction of its spatial periodicity, namely, the transverse $x$ direction in the current work. Such frequency-dependent motion of the output patterns advocates the formation of an instantaneously reconfigurable moving photonic lattice. In the meantime, the readily tunable moving speed determined by the frequency difference also provides a new degree of freedom to manipulate the discrete behaviors of light beam propagation.

The experimental scheme is illustrated in Fig. 1(a). Two laser fields co-propagate inside an atomic vapor cell to suppress the first-order Doppler effect, and an EIT window can be effectively generated in the driven $\Lambda$-type atomic configuration shown in Fig. 1(b). The three-level atomic setting is composed of the hyperfine states $F=2$ (level $|0\rangle$) and $F=3$ ($|2\rangle$) of the ground state $5S_{1/2}$, and one excited state $5P_{1/2}$ ($|1\rangle$) of $^{85}$Rb atoms. The coupling field connecting the transition $|2\rangle \rightarrow |1\rangle$ is a standing wave formed by two elliptical Gaussian coupling beams $\boldsymbol{E}_2$ (frequency $\omega_2$, Rabi frequency $\Omega_2$, wavelength $\lambda_2 \approx 795.0$ nm) and $\boldsymbol{E}_2'$ ($\omega_2'$, $\Omega_2'$) from the same external cavity laser diode. They are arranged to propagate in the same angle of $\theta = 0.25°$ with respect to the $z$-axis and intersect at the center of the vapor cell to establish an interference pattern in the transverse $x$ direction. One coupling beam $\boldsymbol{E}_2'$ is set to pass through two acoustic optical modulators (AOMs) successively to obtain small frequency modification. The first AOM provides a frequency shift of ~200 MHz, while the second AOM gives a shift of approximately −200 MHz in a double-pass configuration, which guarantees a constant output direction of the required $\boldsymbol{E}_2'$ when the frequency shift changes. As a result, the frequency difference $\delta = \omega_2' - \omega_2$ between the two coupling components can be tuned in the range of 0 to 1 MHz, necessary for the generation of the moving lattice. With the Gaussian probe field $\boldsymbol{E}_1$ ($\omega_1$, $\lambda_1 \approx 795.0$ nm, driving the transition $|0\rangle \rightarrow |1\rangle$) from the other ECDL injected into the lattice, a discrete diffraction patterns with the same period as the standing-wave coupling field can occur around the EIT window, requiring the two-photon resonance condition $\Delta_1 - \Delta_1 = 0$ [6,31]. The transmitted probe field is monitored by a charge-coupled device camera.

The probe beam experiences discrete behaviors because it can be confined at the lattice sites (individual waveguide channels) of the electromagnetically induced photonic lattice, which is accomplished by engineering the periodic refractive index with a high nodes–antinodes contrast. Such spatially modified refractive index as a function of the transverse coordinate $x$ is caused by the periodical modulation of the coupling field intensity from the two-beam interference. The refractive index is given as $n = [1+\chi^{(1)}]^{1/2} \approx 1+\chi^{(1)}/2$, and by considering that $n = n_0 + \Delta n$, where $n_0 = 1$ is the background index of the atomic medium and $\Delta n$ is the refractive index modulation arising from the coupling field, the refractive index modulation in the current EIT system is $\Delta n \approx \chi^{(1)}/2$.

Theoretically, the first-order susceptibility of the EIT medium is expressed as $\chi^{(1)} = iN|\mu_{10}|^2[\hbar\varepsilon_0(d_{10}+|\Omega_2 + \Omega_2'|^2/d_{20})]^{-1}$ [23], where $N$ is the atomic density; $\Omega_l = \mu_{ij}E_l/\hbar$ is the Rabi frequency of a transition $|i\rangle \rightarrow |j\rangle$, with $E_l$ being the electric field from the laser beam and $\mu_{ij}$ being the electric dipole momentum ($i$, $j$, and $l$ being integer numbers); $d_1 = \Gamma_{10} + i\Delta_1$ and $d_{20} = \Gamma_{20} + i(\Delta_1 - \Delta_2)$, with $\Gamma_{ij}$ defined as the decay rate between the energy levels $|i\rangle$ and $|j\rangle$. Considering the frequency difference $\delta$ between the two coupling beams, the standing wave acting as the coupling field $\boldsymbol{E}_c$ can be written as

$$|\Omega_2 + \Omega_2'|^2 = (\mu_{12}/\hbar)^2\left[E_2^2 + E_2'^2 + 2E_2E_2'\cos(\delta t + 2k_c x)\right], \quad (1)$$

where $k_c = (k_2 + k_2')(\sin\theta)/2$, with $k_2$ ($k_2'$) defined as the wave vector of $\boldsymbol{E}_2$ ($\boldsymbol{E}_2'$). Clearly, when the two coupling beams have no frequency difference ($\delta = 0$), the interference term $|\Omega_2 + \Omega_2'|^2$ can exhibit a periodic intensity distribution along the transverse $x$ direction, as shown in Fig. 2(a), where the photonic lattice channels always keep parallel to the $z$-axis. Such a standing-wave coupling field can lead to the spatially periodic distribution of the susceptibility under the EIT condition, and an immediately reconfigurable photonic lattice (an exact static lattice) is effectively induced in the atomic vapor. In addition, the probe beam will propagate along the $z$-axis. However, for $\delta \neq 0$, the lattice waveguides gradually depart the $z$-axis at a transverse speed $v = -\delta/2k_c$ during propagation, and a moving lattice is formed. If $\delta$ is constant, the lattice moves along $x$ at a fixed speed. When $\delta$ is positive and negative, the lattice will move along $+x$ and $-x$, respectively [Figs. 2(b) and 2(c)]. Note that since the frequency difference $\delta$ is much smaller than $\omega_2$, the variation of $\delta$ affects $k_c$ negligibly. Further, if $\delta$ increases linearly with time $t$, i.e., $\delta = \alpha t$ (where $\alpha$ is the measure of acceleration), theoretically, the lattice will move along $x$ at a linearly increasing speed and will exhibit a parabolic trajectory inside the atomic vapor along the propagation direction [24]. However, in experiment, due to the limited length of the medium and high speed of light, the curvature of the parabolic lattice can be so small that demonstrating unique features of bending lattices is quite challenging.

The transport dynamics of the probe field $\boldsymbol{E}_1$ inside the moving lattice is governed by the Schrödinger-like equation [32,33]:

$$i\frac{\partial}{\partial z}\boldsymbol{E}_1(x,z) = -\frac{1}{2k_1}\frac{\partial^2}{\partial x^2}\boldsymbol{E}_1(x,z) - \frac{k_1}{2}\chi^{(1)}\boldsymbol{E}_1(x,z), \quad (2)$$

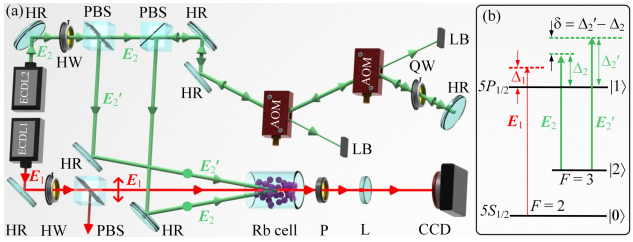


**Fig. 1.** (a) Experimental setup. The polarizations of the probe beam $\boldsymbol{E}_1$ and coupling beams $\boldsymbol{E}_2$ and $\boldsymbol{E}_2'$ are perpendicular, and double-headed arrows and filled dots represent horizontal and vertical polarizations of the beams, respectively. HW, half-wave plate; QW, quarter-wave plate; HR, high-reflectivity mirror; PBS, polarization beam splitter; BS, beam splitter; CCD, charge-coupled device camera; AOM, acoustic optical modulator; P, polaroid; L, lens; LB, light barrier. The standing-wave coupling field exhibits a periodicity of $d = \lambda_2/(2\sin\theta) \approx 91$ μm along the transverse $x$ direction. The 7.5-cm-long atomic cell is wrapped by $\mu$-metal sheets and a heat tape, to shield magnetic fields and control the atomic density, respectively. (b) Three-level $\Lambda$-type atomic configuration. There is a small frequency difference $\delta$ between $\boldsymbol{E}_2$ and $\boldsymbol{E}_2'$. The term $\Delta_1$ (resp. $\Delta_2$ or $\Delta_2'$) denotes the frequency detuning between the resonant frequency for transition $|0\rangle \rightarrow |1\rangle$ (resp. $|2\rangle \rightarrow |1\rangle$) and the frequency of $\boldsymbol{E}_1$ (resp. $\boldsymbol{E}_2$ or $\boldsymbol{E}_2'$).

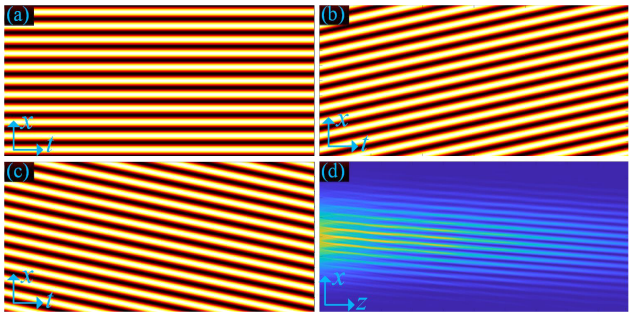


**Fig. 2.** Schematic diagrams of optical lattices inside the medium with the frequency difference set as (a) $\delta = 0$, (b) $\delta = -1$ MHz, and (c) $\delta = 1$ MHz. (d) Simulated propagation behaviors of the Gaussian probe field inside the moving lattice with $\delta = 1$ MHz, $\Delta_1 = 0$, and $\Delta_2 = -10$ MHz.

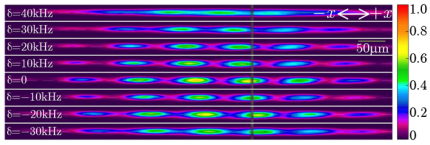


**Fig. 3.** Output patterns of the probe beam (captured at the output surface of the vapor cell by a CCD camera) depicting different moving lattice waveguides, for different $\delta$ values.

where $\boldsymbol{E}_1$ is the electric-field envelope of the incident probe beam, and $k_1 = 2\pi n_0/\lambda_1$ is the wavenumber with $n_0 = 1$ being the background refractive index. The simulated propagating dynamics of the probe beam in a moving lattice is shown in Fig. 2(d), which demonstrates that the probe beam travelling inside the lattice gradually departs from the initial $x$ position and experiences an oblique trajectory in the $(x,\ z)$ plane.

We first observe the propagation of the probe beam in the moving lattice at different speeds via the frequency difference $\delta$. By launching the Gaussian probe beam into the coupling lattice, a clear discrete light pattern can be observed at the output plane of the cell with the two-photon detuning $\Delta_1 - \Delta_2$ ranging from $-30$ MHz to 30 MHz. Figure 3 depicts the output distributions of the probe field for different $\delta$ values. In experiment, by adjusting the controlling voltage on the driver of the double-pass AOM for coupling beam $\boldsymbol{E}_2'$, $\Delta_2'$ is set to make $\delta = \Delta_2' - \Delta_2$ discretely change from $-30$ kHz to 40 kHz with $\Delta_1 - \Delta_2 = 10$ MHz at $\Delta_2 = 0$. Compared to the situation of $\delta = 0$, the output diffraction patterns at positive and negative $\delta$ values move along respective $-x$ and $+x$ directions, and the displacement is more obvious for larger $|\delta|$. This observation is easily understood if one recalls that $v = -\delta/2k_c$, so that the photonic lattice moves in opposite directions for $\delta > 0$ and $\delta < 0$, as the simulation is shown in Figs. 2(a)–2(c), and the bigger $|\delta|$ results in a higher speed $v$, as well as in larger displacement along $x$ for the same propagating length. Excellent agreement between the observations shown in Fig. 3 and the theoretical explanation indicates that frequency difference $\delta$ can certainly give rise to a moving photonic lattice, to guide the discrete propagation dynamics of the incident probe beam.

Another advantage of such induced photonic lattice based on atomic coherence is that the increase of atomic density (determined by the temperature of the atomic sample) is translated directly into the extension of the propagation path length of the probe beam inside the lattice [34]. Thus, increasing the temperature of the medium allows us to easily detect detailed dynamical behaviors of the probe beam inside a moving photonic lattice.

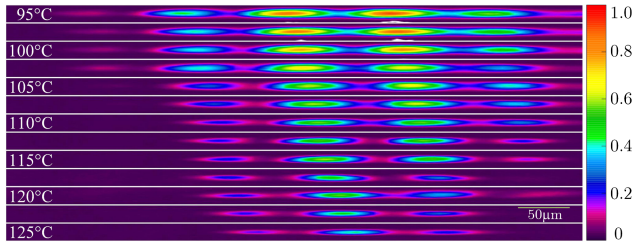


**Fig. 4.** Observed propagation dynamics of a Gaussian probe beam inside the moving lattice with $\delta = -65$ kHz. For the top-to-bottom sequence, the panels demonstrate the output probe patterns by increasing atomic temperature.

As shown in Fig. 4, by adding proper voltages to the two AOM drivers for $\boldsymbol{E}_2'$, to make the frequency difference fixed at $\delta = -65$ kHz, we increase the temperature of the medium from 95°C to 125°C and observe the transport dynamics of the probe beam. Apparently, the output discrete pattern moves uniformly along the $x$-axis, and the transverse displacement increases with the rising of the atomic temperature (denoting the expansion of travelling distance), which agrees well with the predictions shown in Fig. 2(c), where the discrete patterns gradually get far away from the $z$-axis with the expansion of propagation distance. The observations advocate that the photonic lattice has acquired a transverse speed, namely, realizing a moving optical lattice with a readily tunable speed established via atomic coherence.

In summary, in this Letter, we have experimentally demonstrated the discrete propagation dynamics in an easily reconfigurable moving photonic lattice induced in an EIT atomic system. The induced moving photonic lattice, regulated by the frequency difference between the two beams "writing" the lattice in the atomic system, provides a unique platform for manipulating the discrete behaviors of light in a periodic environment. Furthermore, the moving lattice can potentially exhibit accelerating behaviors by linearly increasing (chirping) the frequency difference between the two coupling beams. Actually, from the viewpoint of experiment, the improvement in the linewidth of coupling laser beams can result in a clear interference fringe for a larger frequency difference, far beyond hundreds of KHz (limited by the ~1 MHz linewidth of the laser sources) adopted in the current work. A larger frequency difference can lead to a higher moving speed, and the accelerating characteristics of the moving lattices may become more apparent. Therefore, the current work paves the way for demonstrating the predictions such as optical Bloch oscillation, Zener tunneling [24], and light scattering [35] in accelerating lattices.

**Funding.** National Key Research and Development Program of China (2018YFA0307500, 2017YFA0303703); National Natural Science Foundation of China (62022066, 12074306, 61975159).

**Acknowledgment.** The authors acknowledge helpful discussions with Dr. Yiqi Zhang.

**Disclosures.** The authors declare no conflicts of interest.

**Data Availability.** Data underlying the results presented in this Letter are not publicly available at this time but may be obtained from the authors upon reasonable request.

## REFERENCES


1. I. L. Garanovich, S. Longhi, A. A. Sukhorukova, and Y. S. Kivshar, Phys. Rep. **518**, 1 (2012).
2. S. Longhi, Laser Photon. Rev. **3**, 243 (2009).
3. P. Windpassinger and K. Sengstock, Rep. Prog. Phys. **76**, 086401 (2013).
4. S. Q. Xia, K. Dimitrios, D. H. Song, K. Ioannis, J. J. Xu, A. Szameit, H. B. Buljan, G. M. Konstantinos, and Z. G. Chen, Science **372**, 72 (2021).
5. A. L. M. Muniz, M. Wimmer, A. Bisianov, U. Peschel, R. Morandotti, P. S. Jung, and D. N. Christodoulides, Phys. Rev. Lett. **123**, 253903 (2019).
6. Z. Y. Zhang, Y. Q. Zhang, J. T. Sheng, L. Yang, M.-A. Miri, D. N. Christodoulides, B. He, Y. P. Zhang, and M. Xiao, Phys. Rev. Lett. **117**, 123601 (2016).
7. S. Stutzer, Y. Plotnik, Y. Lumer, P. Titum, N. L. Lindner, M. Segev, M. C. Rechtsman, and A. Szameit, Nature **560**, 461 (2018).
8. L. J. Maczewsky, M. Heinrich, M. Kremer, S. K. Ivanov, M. Ehrhardt, F. Martinez, Y. V. Kartashov, V. V. Konotop, L. Torner, D. Bauer, and A. Szameit, Science **370**, 701 (2020).
9. M. A. Bandres, S. Wittek, G. Harari, M. Parto, J. Ren, M. Segev, D. N. Christodoulides, and M. Khajavilchan, Science **359**, eaar4005 (2018).
10. P. Wang, Y. Zheng, X. Chen, C. Huang, Y. V. Kartashov, L. Torner, V. V. Konotop, and F. Ye, Nature **577**, 42 (2020).
11. R. A. Vicencio, C. Cantillano, M.-I. Luis, B. Real, M.-C. Cristian, S. Weimann, S. Szameit, and M. I. Molina, Phys. Rev. Lett. **114**, 245503 (2015).
12. Z. Y. Zhang, R. Wang, Y. Q. Zhang, Y. V. Kartashov, F. Li, H. Zhong, H. Guan, K. Gao, F. L. Li, Y. P. Zhang, and M. Xiao, Nat. Commun. **11**, 1902 (2020).
13. N. Jiho, S. Huang, P. C. Kevin, and C. R. Mikael, Phys. Rev. Lett. **120**, 063902 (2018).
14. H. Zhong, Y. Q. Zhang, Y. Zhu, D. Zhang, C. B. Li, Y. P. Zhang, F. L. Li, M. R. Belic, and M. Xiao, Ann. Phys. **529**, 1600258 (2017).
15. W. C. Yan, H. Zhong, D. H. Song, Y. Q. Zhang, S. Q. Xia, L. Q. Tang, D. Leykam, and Z. G. Chen, Adv. Opt. Mater. **8**, 1902174 (2020).
16. S. Weimann, M.-I. Luis, B. Real, C. Cantillano, A. Szameit, and R. A. Vicencio, Opt. Lett. **41**, 2414 (2016).
17. G. Benoît and G. B. George, Phys. Rev. B **95**, 165131 (2017).
18. Q. D. Fu, P. Wang, C. M. Huang, Y. V. Kartashov, L. Torner, V. V. Konotop, and F. W. Ye, Nat. Photonics **14**, 663 (2020).
19. E. Lustig, S. Weimann, Y. Plotnik, Y. Lumer, M. A. Bandres, A. Szameit, and M. Segev, Nature **567**, 356 (2019).
20. S. Laxmi and S. K. Awasthi, Physica B **597**, 412360 (2020).
21. H. Qu, Z. Deck-Léger, C. Caloz, and M. Skorobogatiy, J. Opt. Soc. Am. B **33**, 1616 (2016).
22. D. W. Wang, H. T. Zhou, M. J. Guo, J. X. Zhang, J. Evers, and S. Y. Zhu, Phys. Rev. Lett. **110**, 093901 (2013).
23. M. Xiao, Y. Li, S. Jin, and J. Gea-Banacloche, Phys. Rev. Lett. **74**, 666 (1995).
24. Y. Q. Zhang, D. Zhang, Z. Y. Zhang, C. B. Li, Y. P. Zhang, F. L. Li, M. R. Belic, and M. Xiao, Optica **4**, 571 (2017).
25. Z. Zhang, L. Yang, J. Feng, J. Sheng, Y. Zhang, Y. Zhang, and M. Xiao, Laser Photon. Rev. **12**, 1800155 (2018).
26. Z. Zhang, F. Li, G. Malpuech, Y. Zhang, O. Bleu, S. Koniakhin, C. Li, Y. P. Zhang, M. Xiao, and D. D. Solnyshkov, Phys. Rev. Lett. **122**, 233905 (2019).
27. Z. Zhang, S. Liang, F. Li, S. Ning, Y. Li, G. Malpuech, Y. Zhang, M. Xiao, and D. Solnyshkov, Optica **7**, 455 (2020).
28. J. Yuan, S. Dong, H. Zhang, C. Wu, L. Wang, L. Xiao, and S. Jia, Opt. Express **29**, 2712 (2021).
29. J. P. Yuan, C. H. Wu, L. R. Wang, G. Chen, and S. T. Jia, Opt. Lett. **44**, 4123 (2019).
30. J. P. Yuan, S. C. Dong, C. H. Wu, L. R. Wang, L. Xiao, and S. T. Jia, Opt. Express **28**, 23820 (2020).
31. J. T. Sheng, J. Wang, M.-A. Miri, D. N. Christodoulides, and M. Xiao, Opt. Express **23**, 19777 (2015).
32. H. Michinel, M. J. Paz-Alonso, and V. M. Pérez-García, Phys. Rev. Lett. **96**, 023903 (2006).
33. C. Hang, G. Huang, and V. V. Konotop, Phys. Rev. Lett. **110**, 083604 (2013).
34. V. Boyer, C. F. McCormick, E. Arimondo, and P. D. Lett, Phys. Rev. Lett. **99**, 143601 (2007).
35. O. Tetsuyuki and S. Kazuaki, Phys. Rev. B **72**, 205105 (2005).